Published in final edited form as:
Biochim Biophys Acta. 2014 June ; 1840(6): 2042–2049. doi:10.1016/j.bbagen.2014.02.016.

The first cyclomegastigmane rhododendroside A from *Rhododendron brachycarpum* alleviates HMGB1-induced sepsis

Wei Zhou[a,e,1], **Joonseok Oh**[b,1], **Wonhwa Lee**[c,d], **Soyoung Kwak**[c], **Wei Li**[e], **Amar G. Chittiboyina**[f], **Daneel Ferreira**[b], **Mark T. Hamann**[b], **Seung Ho Lee**[a], **Jong-Sup Bae**[c,*], and **MinKyun Na**[e,**]

[a]College of Pharmacy, Yeungnam University, Gyeongsan, Gyeongbuk 712-749, Republic of Korea

[b]Department of Pharmacognosy and Research Institute of Pharmaceutical Sciences, School of Pharmacy, The University of Mississippi, University, MS 38677, USA

[c]College of Pharmacy, CMRI, Research Institute of Pharmaceutical Sciences, Kyungpook National University, Daegu 702-701 and 700-422, Republic of Korea

[d]BK21 Plus KNU Biomedical Convergence Program, Department of Biochemistry and Cell Biology, School of Medicine, Kyungpook National University, Daegu 702-701 and 700-422, Republic of Korea

[e]College of Pharmacy, Chungnam National University, Daejeon 305-764, Republic of Korea

[f]National Center for Natural Products Research, The University of Mississippi, University, MS 38677, USA

Abstract

Background—Endangered plant species are a vital resource for exploring novel drug prototypes. A Korean endangered plant *Rhododendron brachycarpum* G. Don is a broad-leaved shrub native to northern Korea and central Japan. The high mobility group box 1 protein (HMGB1) could be a specific target for the discovery of novel antiseptic agents.

Methods—Gauge-invariant atomic orbital (GIAO) NMR chemical shift calculations were applied for investigation of stereochemical details with accuracy improved by application of DP4 analysis. In vitro antiseptic mechanisms were investigated utilizing immunofluorescence staining, ELISA and cell–cell adhesion assay. Cecal ligation and puncture (CLP) operation was employed to evaluate in vivo potential alleviating severe sepsis and septic shock.

Results—The first bicyclic megastigmane glucoside rhododendroside A (**1**) along with known megastigmane glucosides (**2–5**) were isolated from the leaves of *R. brachycarpum*. The structure of **1** was established by NMR analysis as well as comparison of the experimental chemical shifts

*Corresponding author. Tel.:+82 53 950 8570; fax: +82 53 950 8557. baejs@knu.ac.kr (J.-S. Bae). **Corresponding author. Tel.:+82 42 821 5925; fax: +82 42 823 6566. mkna@cnu.ac.kr (M. Na).
[1]These authors contributed equally to this manuscript.

with those of computed values employing DP4 application. In the CLP operation model that simulates severe sepsis, rhododendroside A (**1**) improved the survival rate up to 60%.

Conclusions—Our results exhibit that *R. brachycarpum* may produce a unique scaffold that is developed into a drug lead mitigating HMGB1-induced vascular pro-inflammatory stimuli and thus alleviating severe sepsis and related manifestations.

General significance—Discovery of new drug leads would warrant conservation efforts of endangered species.

Keywords

Rhododendron brachycarpum; Endangered species; Nuclear magnetic resonance chemical shift calculations; High mobility group box 1 protein; Sepsis

1. Introduction

Endangered plant species are an important resource for exploring novel drug prototypes [1]. A phylogenetic study on the productivity of drug-like molecules reveals that the Viridiplantae kingdom possesses 66 drug-productive families including 61 families gathered in 11 drug-producing clusters [2]. Most of these clustered drug-producing families contain endangered species [2], thus emphasizing the need to protect these fragile plants because their extinction may result in the permanent loss of prospective drug leads. *Rhododendron brachycarpum* G. Don (Ericaceae) is a broad-leaved shrub native to northern Korea and central Japan [3]. The numbers of this species have been drastically diminished due to climate change, leading to its classification as an endangered and rare species in Korea [3]. Although *R. brachycarpum* is traditionally employed in the treatment of diseases including cardiovascular, diabetes, hypertension, hepatitis, rheumatoid arthritis, and headache [4], only a limited number of studies have been carried out to validate these ethnopharmacological uses [5,6].

Sepsis is a systemic and overwhelming inflammatory response of an organism to a local infection, potentially progressing to severe sepsis and septic shock with multiple organ failure and hypotension [7]. The mortality associated with the disease is as high as 50–70%, leading to its designation as the number one cause of death in intensive care units worldwide [7]. Comprehensive anti-inflammatory treatments have not alleviated the disease during the last few decades [7]. The only FDA-approved antiseptic drug, drotrecogin alfa (Xigris®), was withdrawn from the market due to its questionable efficacy [8], thus stressing the necessity for the search of potent antiseptic prototypes with novel modes of action (MOA). Among the therapeutic strategies targeting the mitigation of sepsis [7], enhancement of the integrity of endothelial cells (ECs) has emerged as a sensible MOA of an antiseptic drug [9,10]. Disruption of the integrity of ECs facilitates leucocytes to access inflamed tissue and hence initiating such vascular inflammatory manifestations [9,10]. In this regard, high mobility group box 1 (HMGB1) protein could be a specific target for the discovery of novel antiseptic agents capable of achieving vascular barrier augmentation because of the role of the protein in disturbing the barrier integrity of ECs, and ultimately inducing severe sepsis and related manifestations [9–11]. In our continuing efforts aimed at discovering viable and new drug prototypes from endangered species and validating the ethnopharmacological

applications [1,3,4,12], we herein present the isolation and structural characterization of rhododendroside A (**1**), the first bicyclic megastigmane glucoside. We also discuss the potential of this scaffold for the development of a septic drug capable of mitigating HMGB1-induced vascular disruption.

2. Materials and methods

2.1. General procedures

NMR experiments were conducted using a Bruker DMX 250 (^{1}H-250 MHz, ^{13}C-63 MHz), and Bruker DMX 600 (^{1}H-600 MHz, ^{13}C-150 MHz) spectrometers (Karlsruhe, Germany) referenced by residual pyridine and MeOH signals. Optical rotations were recorded using a JASCO DIP-1000 (Tokyo, Japan) and mass spectrometric data were obtained utilizing a SYNAPT G2 Waters mass spectrometer (Manchester, U.K.). MPLC was carried out employing Biotage Isolera™ reversed phase C_{18} SNAP Cartridge KP-C_{18}-HS and normal phase SNAP Cartridge KP-Sil (340 g, Biotage AB, Uppsala, Sweden). The gas chromatography (GC) analysis was carried out on a Shimadzu-2010 with an SPB-1 column (0.25 mm × 30 m, temperature: 250 °C) employing flame ionization detector (FID) and helium as carrier gas. HPLC separation was performed using a Gilson system with a UV detector and Phenomenex Luna C_{18} column (250 × 21.2 mm, 10 μm and 250 × 4.60 mm, 5 μm). TLC was performed on glass plates precoated with silica gel 60 F_{254} and RP-18 F_{254} (Merck). Column chromatography was performed using silica gel (Merck, 70–230 mesh).

2.2. Extraction and purification

Leaves of *R. brachycarpum* (Fig. S1) were collected on a farm in Gongju Korea in 2011, identified by Prof. MinKyun Na (College of Pharmacy, Chungnam National University) and deposited at the Pharmacognosy Laboratory of the College of Pharmacy, Chungnam National University, Daejeon, Korea (CNU00195). Dried leaves (25 kg) were extracted with MeOH (2 × 250 L) at room temperature for one week and the extract was concentrated to yield a brownish slurry (6 kg). Half of the extract (3 kg) was suspended in H_2O (10 L) and partitioned with *n*-hexane (10 L × 3), $CHCl_3$ (10 L × 3), EtOAc (10 L × 3), and BuOH (10 L × 3) to afford four extracts amounting to 438, 140, 450 and 320 g, respectively. The BuOH-fraction (320 g) was further subjected to silica gel column VLC and eluted with CH_2Cl_2:MeOH:H_2O (10:1 → 2:1:0.1) to obtain six fractions (Fr. B1–B6). Fr. B1 (10 g) was purified by MPLC (C_{18} SNAP Cartridge KP–C_{18}–HS, 340 g) eluting with MeOH:H_2O (3:7→7:3) to afford seven sub-fractions (Fr. B11–B17). Fr. B14 (1.46 g) was further purified employing preparative HPLC (Luna C18(2) column: 250 × 21.20 mm, 20% MeCN, flow rate: 6 ml/min) to afford compounds **2** (26 mg, t_R 40.2 min) and **5** (3.8 mg, t_R 53.6 min). Fr. B2 (22 g) was fractionated into nine fractions (B21–B29) utilizing MPLC (C_{18} SNAP Cartridge KP–C_{18}–HS, 340 g, column) eluting with acetone:MeOH:H_2O (0:0:100 → 12:28:60). Fr. B26 (1.7 g) was subjected to silica gel MPLC (SNAP Cartridge KP-Sil, 120 g) and eluted with EtOAc:MeOH (98:2 → 90:10) to yield five fractions (B261–B265). Fr. B262 (92 mg) was chromatographed over a silica gel column (2 × 80 cm) and eluted with $CHCl_3$:acetone:H_2O (1:2:0.1) to get compound **1** (2 mg). Compound **4** (34 mg) was acquired from Fr. B264 (120 mg) using a silica gel column (2 × 80 cm) eluting with $CHCl_3$:MeOH:H_2O (6.5:1:0.1). Fr. B27 (2 g) was subject to silica gel MPLC (SNAP

Cartridge KP-Sil, 120 g) and eluted with $CHCl_3$:MeOH (94:6 → 85:15) to yield compound **3** (159 mg). The known megastigmane glucosides, picrionoside A (**2**) [13], icariside B_2 (**3**) [14], citroside A (**4**) [15] and icariside B_6 (**5**) [14] were identified by 1D and 2D NMR analysis and confirmed by comparing the physical and spectroscopic data with those in the literature ($[\alpha]_D^{25}$, MS and NMR) (Supplementary data 1).

2.2.1. Rhododendroside A (1)—Rhododendroside A (**1**): yellow amorphous powder; $[\alpha]_D^{20}$: −15.4 (*c* 0.1, MeOH); HR-ESI-MS: *m/z* 411.1996 $[M + Na]^+$ (calcd. for $C_{19}H_{32}O_8Na$, 411.1995). ^1H NMR (methanol-d_4, 600 MHz) and ^{13}C-NMR (methanol-d_4, 150 MHz) data, see Table 1.

With reference to a previous study [16], the acid hydrolysis of compound **1** was performed as follows; the compound was heated in 10% HCl (1 mL) at 85 °C for 3 h and the residue was partitioned with EtOAc and H_2O. The aqueous layer was evaporated to yield a residue and the residue was dissolved in anhydrous pyridine (100 μL) followed by the addition of 0.1 ML-cysteine methyl ester hydrochloride (100 μL). After heating at 60 °C for 1.5 h, the residue was dried and trimethylsilylated with the addition of 1-trimethylsilylimidazole solution (500 μL), and heated at 60 °C for 5 min. The dried product was partitioned with *n*-hexane and H_2O, and the non-polar layer was analyzed using GC technique. The monosaccharide moiety was confirmed as D-glucose based on comparison of the retention time with that of a D-glucose standard (t_R 16.21 min, see Fig. S1–13).

2.3. GIAO NMR chemical shift (CS) calculations [17,18]

All conformational searches were achieved employing Macromodel (Version 9.9, Schrodinger LLC.) program with “Mixed torsional/Low Mode sampling” in MMFF force field. The searches were performed in the gas phase with a 50 kJ/mol energy window limit and 10,000 maximum number of steps to completely investigate all low-energy conformers. All minimization processes were accomplished utilizing Polak–Ribiere Conjugate Gradient (PRCG) method, 10,000 maximum iterations and a 0.001 kJ (mol Å)$^{-1}$ convergence threshold on the rms gradient. C-2–C-3 and C-3–C-4 bonds in compound **1** were constrained using a 1,000 force constant based on the associated coupling constants [$^3J_{H\text{-}2ax,H\text{-}3}$ (12.6 Hz), $^3J_{H\text{-}3,H\text{-}4ax}$ (12.6 Hz)]. Conformers within 10 kJ/mol of each global minimum of the two diastereomers (diastereomers **I** and **III** shown in Fig. 2B) were selected for GIAO shielding constants calculation without geometry optimization employing Gaussian 09 package (Gaussian Inc.) at the B3LYP/6-31G(d,p) level in the gas phase. Calculated chemical shift (CS) values were obtained according to the following equation:

$\delta^x_{calc.} = \frac{\sigma^0 - \sigma^x}{1 - \sigma^0/10^6}$ in which $\delta^x_{calc.}$ is the calculated CS value for nucleus *x* (e.g., 1H or 13C), σ^x and σ^0 are the calculated isotropic constants for nucleus *x* and tetramethylsilane (TMS), respectively. The geometry of TMS was optimized using the B3LYP/6-31G(d,p) level in the gas phase using Gaussian 09 package (Gaussian Inc.) for unbiased comparison of calculated CS values with those of other molecules according to the original author’s recommendation [18]. These calculated chemical shift values were Boltzmann-averaged based on their relative MMFF94 potential energy (see Table S1-1) and these averaged values were used for the calculation of DP4 probability employing an applet available at http://www-

jmg.ch.cam.ac.uk/tools/nmr/DP4/. In utilizing DP4 analysis, the assignment of diastereotopic protons and carbons was accomplished based on the associated NOE correlations and coupling constants (Fig. S1–14), and computed and experimental CS values of each nucleus were compared using DP4 analysis. All 3D images in the manuscript and Supplementary data were rendered utilizing Pymol 1.6.x (Schrödinger LLC.).

3. Results and discussion

An extract of the leaves of *R. brachycarpum* (Fig. S1-1) was fractionated and purified employing various chromatographic techniques (see *2.2. Extraction and purification*), leading to the purification of megastigmane glucosides (**1–5**) (Fig. 1A). Compound **1** was obtained as a yellow amorphous powder and the molecular formula was established as $C_{19}H_{32}O_8$ based on HR-ESI-MS data (obsd. $[M + Na]^+$, *m/z* 411.1996; calcd. $[M+Na]^+$, *m/z* 411.1995). The ^1H NMR spectrum (Table 1) displayed resonances for an olefinic proton (δ_H 4.51), an anomeric proton (δ_H 4.43), an oxymethine proton (δ_H 4.16), an allylic (δ_H 1.66) and three tertiary methyl groups (δ_H 1.30, 1.07, 1.03). The ^{13}C NMR spectrum (Table 1) exhibited 19 resonances including six carbon resonances belonging to a glucopyranosyl moiety (δ_C 102.8, 75.1, 78.0, 71.6, 77.8, 62.7), two olefinic carbons (δ_C 149.4, 97.6), an oxymethine carbon (δ_C 73.2), three quaternary carbons (δ_C 81.5, 72.0, 40.7), three methylene carbons (δ_C 44.7, 41.4, 29.9), one allylic (δ_C 20.0), and three tertiary methyl carbons (δ_C 27.4, 24.6, 22.7). These spectroscopic data are similar to those of icariside B_2 (**3**) [14], indicating the presence of a megastigmane glucoside framework in **1**. Differences in the NMR data of **3** and **1** include the disappearance of the proton signals of the conjugated *trans*-olefinic group and a change of the nature of the acetylmethyl group in **3** compared to **1**. These differences are compatible with a structure of **1** generated from **3** via cyclization of the C-6 methyl vinyl ketone functionality onto the oxirane moiety. This was confirmed by HMBC correlations between H-8 (δ_H 4.51) and C-6 (δ_C 72.0), C-7 (δ_C 29.9), C-9 (δ_C 149.4), and C-10 (δ_C 20.0), and between H-7 (δ_H 2.34, 1.99) and C-6 (δ_C 72.0), C-8 (δ_C 97.6), and C-9 (δ_C 149.4) (Fig. 1B). Such formation of a hexahydro-4 *H*-chromenemoiety and thus a unique cyclomegastigmane scaffold has not previously been observed. The connectivity of the aglycone and monosaccharide moieties was confirmed by an HMBC correlation between H-1′ (δ_H 4.43) and C-3 (δ_C 73.2) (Fig. 1B). The coupling constant (*J*=7.8Hz) of the anomeric proton confirmed a *β*-glucosidic linkage. Acid hydrolysis followed by GC analysis (see Fig. S1–13) confirmed the presence of D-(+)-glucose.

The relative configuration of the aglycone was established via coupling constants and NOE correlations. The coupling constants of H-3 (tt, 12.6, 4.1 Hz) suggest that the cyclohexane ring occupies either a chair (diastereomer **I**) or boat conformation (diastereomer **II**) (Fig. 2A). The relative configuration of C-5 was assigned based on the presence of a strong NOE correlation between H-3 (δ_H 4.16) and H-12 (δ_H 1.07) and the absence of an NOE correlation between H-3 (δ_H 4.16) and H-13 (δ_H 1.30) (Fig. 2A). Based on these findings, two plausible diastereomers (**I**: 3*S*, 5*R*, 6*R*; **II**: 3*S*, 5*R*, 6*S*) were proposed and minimized with the aforementioned dihedral constraints and spatial distance information employing the MMFF94 force field (Schrödinger LLC.) (Fig. 2A). The presence of an NOE correlation between H-12 (δ_H 1.07) and H-8 (δ_H 4.51) in diastereomer **I** and the absence of an NOE correlation between H-11 (δ_H 1.03) and H-13 (δ_H 1.30), but feasible in diastereomer **II**,

support the relative configuration of diastereomer **I** and confirmits structural equivalence with compound **1** (Fig. 2A). Owing to the mass limitations of **1**, definition of the absolute configuration was attempted utilizing gauge-invariant atomic orbital (GIAO) NMR chemical shift (CS) calculations with accuracy improved by application of DP4 analysis that has been successfully applied for investigation of such stereochemical details [17–19]. Having established the D-glucopyranosyl moiety in **1**, diastereomers **I** and **III** with enantiomeric aglycone moieties were considered (Fig. 2B). The major conformers of diastereomers **I** and **III,** generated by conformational searches employing Macromodel (Schrodinger LLC.), were subjected to GIAO shielding constant calculations at the B3LYP/6-31G(d,p) level employing the Gaussian 09 package (Gaussian Inc.) (see *2.3. GIAO NMR chemical shift calculations*). The calculated CS values were Boltzmann-averaged based on their relative MMFF94 potential energy (Table S1–2) and these averaged values were used for the calculation of DP4 probability (see *2.3. GIAO NMR chemical shift calculations* and Fig. S1–14). According to DP4 analysis (Table 1), diastereomer **I** was supported with 98.4 % probability when CS values of the two nuclei were taken into consideration, permitting assignment of absolute configuration of compound **1** identical to that showed for diastereomer **I**. Moreover, consistency regarding the 3*S*-configuration among analogs **2–5** [13–15] further supports the DP4 prediction of the 3*S* configuration of **1** when considered in conjunction with a similar biosynthetic pathway towards these bisnorsesquiterpenes. As shown in Fig. 3, enzymatic epoxidation of **5** would stereochemically be directed by the 3*β*-equatorial substituent, leading to formation of oxirane **6** that would be susceptible to successive cyclization and dehydration via **7** to form **1**. On the basis of these findings, the structure of **1** was defined as (3*S*,5*R*,6*R*)-1,1,5,9- tetramethyl-3-*β*-D-glucopyranosyloxy-2,3,4,5-tetrahydro-7*H*-chromen-6-ol, named rhododendroside A (**1**).

Compounds **1–5**, showing vascular barrier protective activity in an HMGB1-mediated permeability test (See Biological Assay Details in Supplementary data 2), were further evaluated for their potential to hamper HMGB1-mediated vascular disruption as cause of severe septic diseases [9,10,20]. To evaluate the actin cytoskeletal arrangement activity of **1–5**, human umbilical vein endothelial cells (HUVECs) were treated with 10 μM of each compound employing immunofluorescence staining of HUVEC monolayers with the F-actin labeled fluorescein phalloidin (Fig. 4A). The control displayed random F-actin distribution throughout cells with actin filament bundles localized at cell boundaries (Fig. 4A) while vascular barrier disruption triggered by HMGB1 (1 μg/mL) was evidenced by the generation of paracellular gaps upon HMGB1 treatment (arrowed in Fig. 4A). Pretreatment with **1**, **2**, and **5** eliminated HMGB1-induced paracellular gaps and facilitated the formation of dense F-actin rings (Fig. 4A), protecting vascular barrier integrity from HMGB1-induced vascular stress, whereas pretreatment with **3** and **4** did not recover the HMGB1-mediated paracellular gaps (Fig. 4A). To further examine if compounds **1–5** enhance barrier integrity of HUVECs, a permeability assay was performed with various concentrations (1–10 μM). Pretreatment with **1**, **2**, and **5** (10 μM) restored the levels of permeability to those of the negative control (Fig. 4B) in HMGB1- stimulated barrier integrity disruption while their pretreatment (10 μM) without the vascular stressor did not influence the barrier integrity, validating their strong supportive action of vascular barrier integrity (Fig. 4B). To verify if the observed barrier protective action was associated with HMGB1 signaling through its receptors,

expression of such receptors, including toll-like receptors 2 and 4 (TLR2, TLR4) and receptor for advanced glycan endproducts (RAGE), was monitored upon pretreatment with compounds **1–5** (1–10 μM). Pretreatment of **1**, **2** and **5** diminished the HMGB1 receptors in a dose-dependent manner, implying that the active compounds exerted the vascular barrier restorative action via the inhibition of HMGB1 interacting with the receptors (Fig. 4C). Phosphorylation of p38 MAPK (mitogen-activated protein kinase)was also evaluated employing enzyme-linked immunosorbent assay (ELISA) based on studies that HMGB1 induces pro-inflammatory response by promoting phosphorylation of p38 [9,10]. The treatment of HUVECs with HMGB1 significantly enhanced phosphorylation of p38 and this up-regulation was attenuated upon the pretreatment with **1**, **2**, and **5**, indicating that they averted HMGB1-induced pro-inflammatory reactions and consequently maintaining vascular barrier integrity (Fig. 4D). HMGB1 mediates inflammatory response through enhancing cell surface expression of cellular adhesion molecules (CAMs) on the surfaces of endothelial cells, such as ICAM-1 (intercellular CAM 1), VCAM-1 (vascular CAM 1), and E-selectin, and thus facilitating adhesion and migration of leukocytes across endothelium to inflamed sites [9,10]. Based on this migration mechanism, HUVECs were treated with compounds **1–5** followed by HMGB 1-induced vascular barrier interruption and expression of the adhesion factors was assessed. Expression of CAMs was heightened upon HMGB 1 treatment (Fig. 4E) and pretreatment with **1**, **2**, and **5** inhibited the up-regulated adhesion factors in a concentration-dependent manner. Successively, cell-cell adhesion assay employing THP-1 cell line was performed given previous studies demonstrating that enhanced expression of CAMs corresponds to escalated binding potential of THP-1 cells to HMGB1-challenged ECs [9,10]. As shown in Fig. 4F, treatment with **1**, **2**, and **5** diminished THP-1 cell adherence toward HMGB1-treated HUVECs in a concentration dependent manner. Overall, these in vitro findings cohesively corroborated the active compounds exerted vascular protective potential via inhibition of HMGB1-induced pro-inflammatory response.

In vivo experiments employing murine models were conducted to confirm the observed in vitro vascular barrier protective effects. Intravenous pretreatment of mice with **1–5** (7.7 μg/mouse) was carried out followed by HMGB1 (2 μg/mouse, i.v.)-induced barrier disruption in vivo. Compounds **1**, **2** and **5** protecting vascular barrier integrity in vitro, also restored vascular permeability in vivo upon HMGB1- induced pro-inflammatory stimuli based on the decreased dye leakage levels to near those of the negative control, while compounds **3** and **4** did not suppress the levels of dye leakage (Fig. 5A). To corroborate in vitro anti-migration effects of the active compounds, in vivo leukocyte migration was evaluated by counting the number of migrated leukocytes into peritoneal cavities upon HMGB1-challeged mice models. As shown in Fig. 5B, intravenous pretreatment with **1**, **2** and **5** inhibited migration of leukocytes based on the decreased peritoneal leukocytes counts, verifying their inhibitory action on leukocytes chemotaxis upon HMGB1-induced inflammatory environment.

To validate if the active megastigmane glucosides are developed into practical antiseptic drug leads inhibiting HMGB1-induced vascular stress, they were administered to mice (7.7 μg/mouse) upon cecal ligation and puncture (CLP) operation employed to simulate severe sepsis and its related manifestations [21]. According to the Kaplan– Meier survival analysis

[9,10], compounds **1**, **2**, and **5**, demonstrating potent vascular barrier protective activity in vitro and in vivo, improved the survival rate to 60, 40, and 40 %, respectively, 132 h after the CLP operation (Fig. 5C). In view of these biological findings, it is plausible that the megastigmane glucosides restore in vitro and in vivo vascular integrity with mitigating HMGB1-induced pro-inflammatory vascular stimuli, ultimately leading to alleviating septic lethality. Thus, megastigmane glucosides (**1**, **2**, and **5**) could be a practical starting point not only for conducting further structure–activity relationship studies but also developing an effective antiseptic agent.

4. Conclusion

Our results demonstrate that *R. brachycarpum* may be the source of a unique scaffold that is developed into an antiseptic lead mitigating HMGB1-induced vascular pro-inflammatory stimuli. These results also reaffirm that rare and endangered plant species offer unique opportunities to explore novel drug leads, warranting conservation efforts especially in cases where modern-day disease challenges are intensifying.

Supplementary Material

Refer to Web version on PubMed Central for supplementary material.

Acknowledgments

We would like to recognize Drs. J. Goodman (U. Cambridge), M. Lodewyk (UC Davis), and T. Lee (Kyungpook National U.) for helpful discussion and technical help, and the Mississippi Center for Supercomputing Research (MCSR) for supercomputer access. This research was supported by Basic Science Research Program through the National Research Foundation of Korea (NRF) funded by the Ministry of Education and the Ministry of Science, ICT and Future Planning (2009-0093815, 2010-0020484, and 2011-0024389).

References

1. Ibrahim MA, Na M, Oh J, Schinazi RF, McBrayer TR, Whitaker T, Doerksen RJ, Newman DJ, Zachos LG, Hamann MT. Significance of endangered and threatened plant natural products in the control of human disease. Proc Natl Acad Sci U S A. 2013; 110:16832–16837. [PubMed: 24082148]
2. Zhu F, Qin C, Tao L, Liu X, Shi Z, Ma X, Jia J, Tan Y, Cui C, Lin J, Tan C, Jiang Y, Chen Y. Clustered patterns of species origins of nature-derived drugs and clues for future bioprospecting. Proc Natl Acad Sci U S A. 2011; 108:12943–12948. [PubMed: 21768386]
3. Choi YH, Zhou W, Oh J, Choe S, Kim DW, Lee SH, Na M. Rhododendric acid A, a new ursane-type PTP1B inhibitor from the endangered plant *Rhododendron brachycarpum* G. Don. Bioorg Med Chem Lett. 2012; 22:6116–6119. [PubMed: 22940448]
4. Bae, KH. The Medicinal Plants of Korea. Kyo-Hak; Seoul: 2000.
5. Choi J, Young H, Park J, Choi JH, Woo W. Further study on the constituents of *Rhododendron brachycarpum*. Arch Pharm Res. 1987; 10:169–172.
6. Youn H, Cho JH. Isolation and structure elucidation of triterpenoidal constituents from the leaves of *Rhododendron brachycarpum*. Kor J Pharmacogn. 1991; 22:18–21.
7. Riedemann NC, Guo RF, Ward PA. Novel strategies for the treatment of sepsis. Nat Med. 2003; 9:517–524. [PubMed: 12724763]
8. Ranieri VM, Thompson BT, Barie PS, Dhainaut JF, Douglas IS, Finfer S, Gårdlund B, Marshall JC, Rhodes A, Artigas A, Payen D, Tenhunen J, Al-Khalidi HR, Thompson V, Janes J, Macias WL, Vangerow B, Williams MD. Drotrecogin alfa (activated) in adults with septic shock. N Engl J Med. 2012; 366:2055–2064. [PubMed: 22616830]

9. Lee W, Kim TH, Ku S-K, Min K-j, Lee H-S, Kwon TK, Bae J-S. Barrier protective effects of withaferin A in HMGB1-induced inflammatory responses in both cellular and animal models. Toxicol Appl Pharmacol. 2012; 262:91–98. [PubMed: 22561332]
10. Yang EJ, Ku SK, Lee W, Lee S, Lee T, Song KS, Bae JS. Barrier protective effects of rosmarinic acid on HMGB1-induced inflammatory responses in vitro and in vivo. J Cell Physiol. 2013; 228:975–982. [PubMed: 23042518]
11. Bae JS. Role of highmobility group box 1 in inflammatory disease: Focus on sepsis. Arch Pharm Res. 2012; 35:1511–1523. [PubMed: 23054707]
12. Zhou W, Oh J, Li W, Kim DW, Lee SH, Na M. Phytochemical studies of Korean endangered plants: a new flavone from *Rhododendron brachycarpum* G. Don. Bull Kor Chem Soc. 2013; 34:2535–2538.
13. Uchiyama T, Nishimura K, Miyase T, Ueno A. Terpenoid glycosides from *Picris hieracioides*. Phytochemistry. 1990; 29:2947–2951.
14. Miyase T, Ueno A, Takizawa N, Kobayashi H, Karasawa H. Studies on the glycosides of *Epimedium grandiflorum* Morr. var. *thunbergianum* (Miq.) Nakai. I. Chem Pharm Bull. 1987; 35:1109–1117.
15. Zhang Z, Zhang W, Ji YP, Zhao Y, Wang CG, Hu JF. Gynostemosides A–E, megastigmane glycosides from *Gynostemma pentaphyllum*. Phytochemistry. 2010; 71:693–700. [PubMed: 20097393]
16. Hara S, Okabe H, Mihashi K. Separation of aldose enantiomers by gas–liquid chromatography. Chem Pharm Bull. 1986; 34:1843–1845.
17. Smith SG, Goodman JM. Assigning the stereochemistry of pairs of diastereoisomers using GIAO NMR shift calculation. J Org Chem. 2009; 74:4597–4607. [PubMed: 19459674]
18. Smith SG, Goodman JM. Assigning Stereochemistry to Single Diastereoisomers by GIAO NMR Calculation: The DP4 Probability. J Am Chem Soc. 2010; 132:12946–12959. [PubMed: 20795713]
19. Lodewyk MW, Tantillo DJ. Prediction of the structure of nobilisitine A using computed NMR chemical shifts. J Nat Prod. 2011; 74:1339–1343. [PubMed: 21469691]
20. Yang H, Ochani M, Li J, Qiang X, Tanovic M, Harris HE, Susarla SM, Ulloa L, Wang H, DiRaimo R, Czura CJ, Wang H, Roth J, Warren HS, Fink MP, Fenton MJ, Andersson U, Tracey KJ. Reversing established sepsis with antagonists of endogenous high-mobility group box 1. Proc Natl Acad Sci U S A. 2004; 101:296–301. [PubMed: 14695889]
21. Rittirsch D, Huber-Lang MS, Flierl MA, Ward PA. Immunodesign of experimental sepsis by cecal ligation and puncture. Nat Protoc. 2008; 4:31–36. [PubMed: 19131954]

Appendix A. Supplementary data

NMR spectra of all compounds, HR-ESI-MS spectrum of compound **1** and computational details (Supplementary data 1), and in vitro and in vivo biological assay details and results of compounds **1**–**5** (Supplementary data 2) can be found online at http://dx.doi.org/10.1016/j.bbagen.2014.02.016.

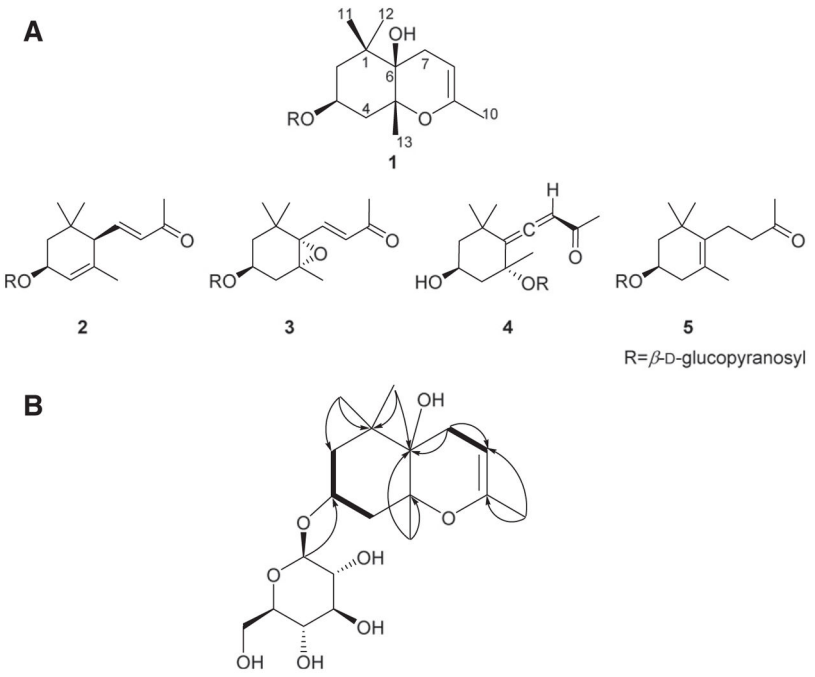

Fig. 1.

Structures of **1–5** from *R. brachycarpum* (A) and key COSY ( ) and HMBC (→) correlations in **1** (B).

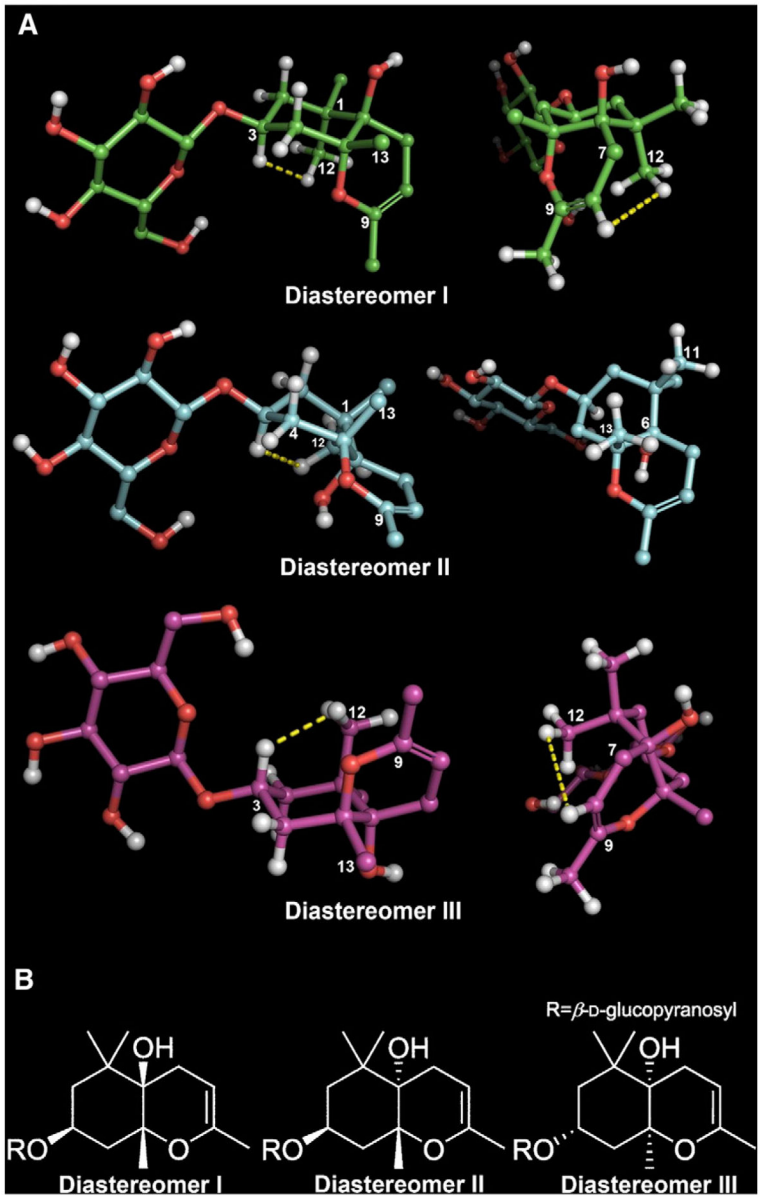

Fig. 2.
Plausible diastereomers of **1** (The yellow dotted lines indicate NOE correlations).

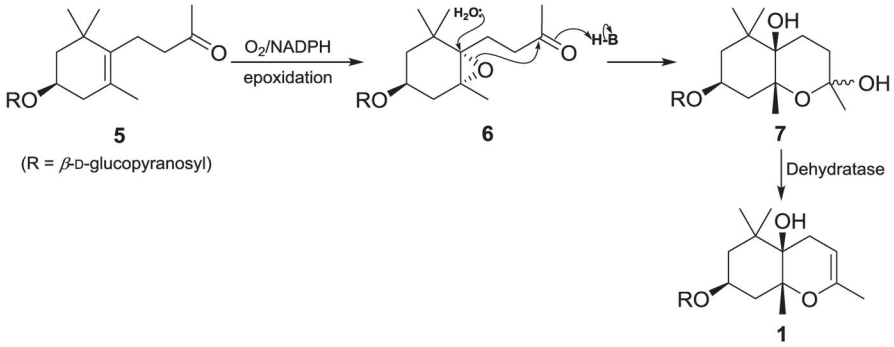

Fig. 3.
Plausible biosynthetic pathway for generation of rhododendroside A (**1**).

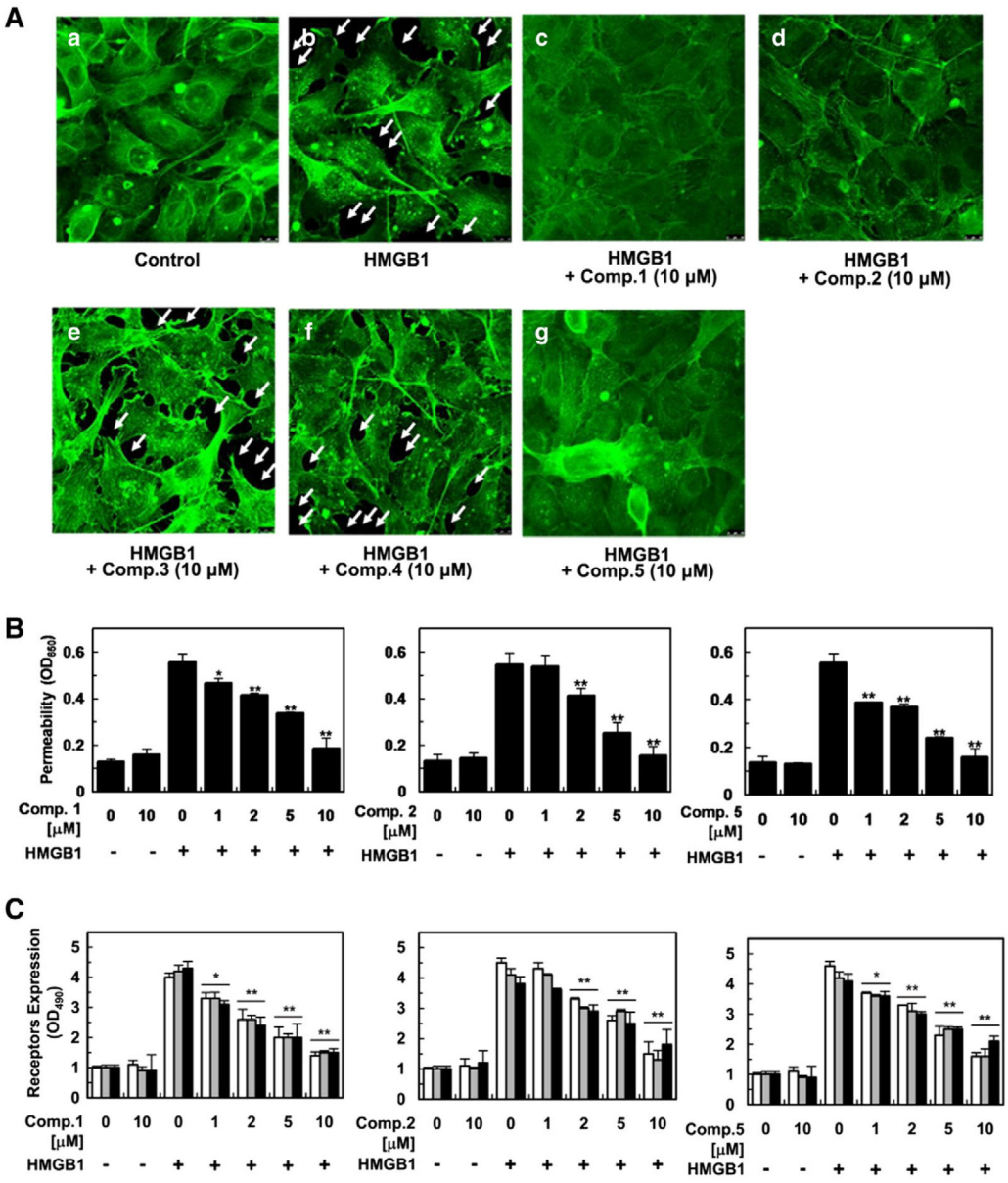

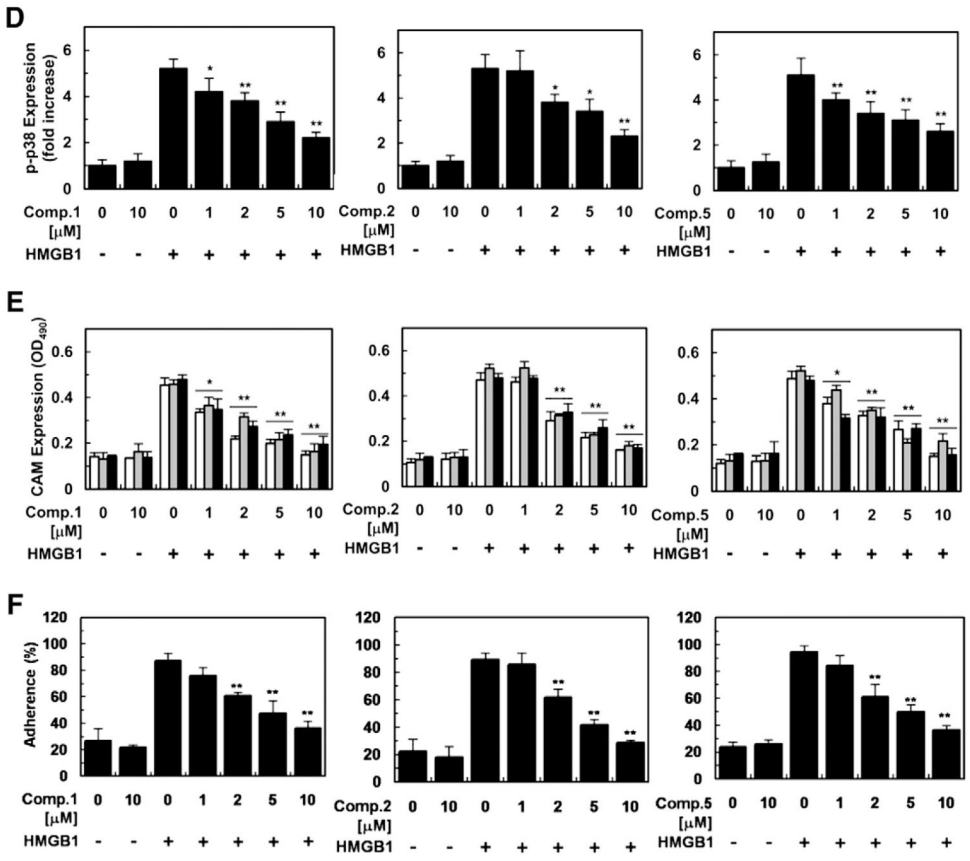

Fig. 4.

In vitro evaluation of vascular protective action of compounds **1**, **2**, and **5** against HMGB1 (1 μg/mL for 16 h)-induced vascular barrier disruption. Data were analyzed upon pretreatment of HUVECs with the indicated concentrations for 6 h. Staining for F-actin upon pretreatment of **1–5** (A). HMGB1-induced permeability was monitored by assessing the flux of Evans blue bound albumin across HUVECs (B). Influence of **1**, **2**, and **5** on expression of HMGB1 receptors (C), phosphorylation of p38 (D), and CAMs (E)was evaluated by ELISA. White, gray, and black bars indicate expression of TLR2, TLR4, and RAGE (C) and VCAM-1, ICAM-1, and E-selectin, respectively (E). Cell adhesion inhibitory action against enhanced cell-cell adhesion by HMGB1-induced vascular stress was assessed utilizing fluorescently labeled THP-1 cells (F). Biological results of inactive compounds (**3**, **4**) are shown in Supplementary data 2. Results are indicated with the means ± SDs of different of at least three experiments and *$p < 0.05$ and **$p < 0.01$ compared to cells only treated with HMGB1 (B–F).

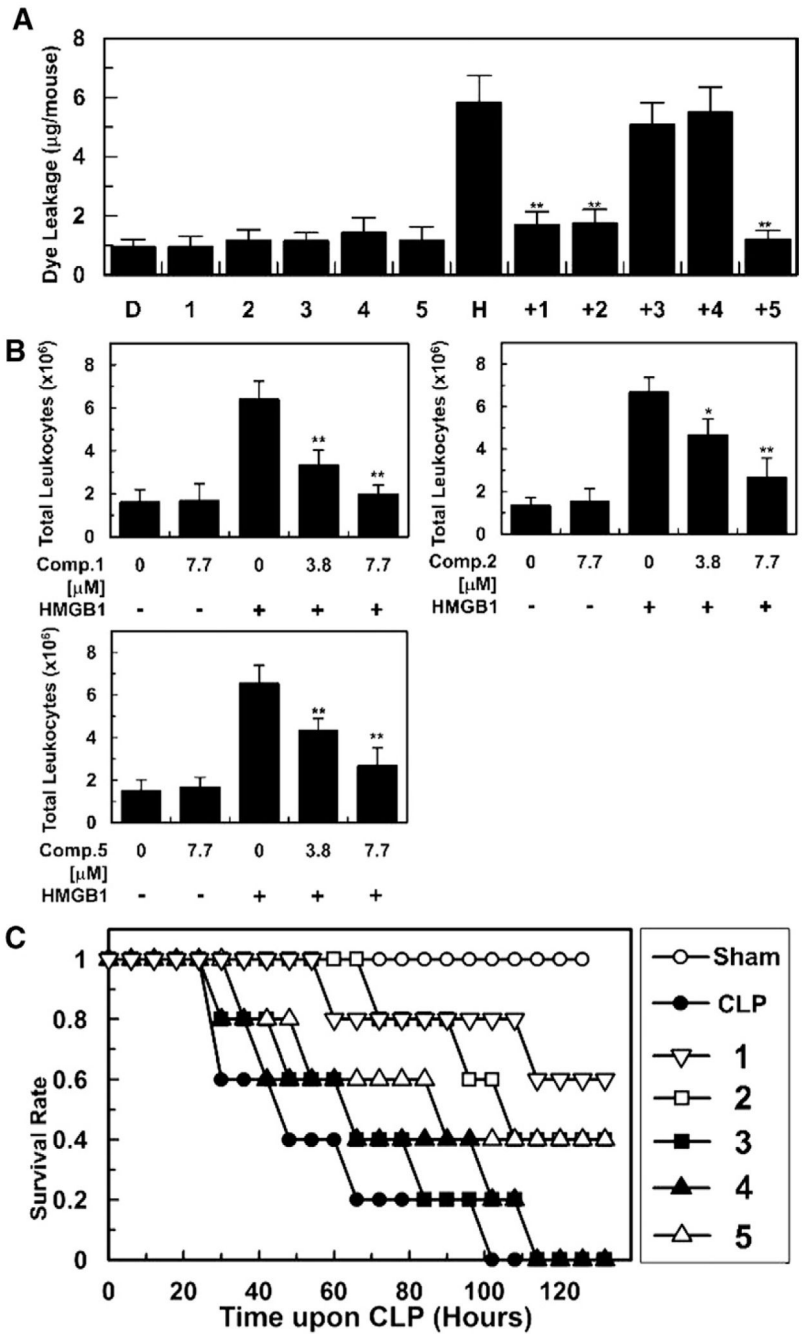

Fig. 5.

In vivo vascular supportive and antiseptic action of **1–5** (7.7 μg/mL) upon HMGB1 (2 μg/mouse, i.v.)-mediated pro-inflammatory environment (A, B) and CLP operation (C). Effects of **1–5** on vascular permeability was measured by the amount of Evans blue in peritoneal washings (n = 5) (A). H and D stand for mice groups administered with HMGB1 and DMSO, respectively (A). Anti-migration (B, n = 5) and anti-lethality activity (C, n = 10) of **1–5** were evaluated by counting the number of migrated leukocytes into peritoneal cavities and using a CLP-induced septic shock mice model, respectively. Control CLP mice (●) and

sham-operated mice (○) were administered sterile saline and survival was monitored every six-hour (C). Biological results of inactive compounds (**3**, **4**) are found in Supplementary data 2. Results are shown with the means ± SDs of three different experiments and *$p < 0.05$ and **$p < 0.01$ compared to mice only treated with HMGB1 (A, B).

Table 1

^{1}H (600 MHz) and ^{13}C (150 MHz) NMR data of compound **1** in methanol-d_4 and calculated CS values of diastereomer **I** and **III.**

^{1}H NMR CS values (δ_H)				^{13}C NMR CS values (δ_C)		
Position[a]	Exp. δ_H, multi, (*J* in Hz)	Cal.			Cal.	
		I[b]	III[c]	Exp.	I[b]	III[c]
1				40.7	44.8	44.5
2ax.	1.76, t, (12.6)	1.90	1.75	44.7	47.7	45.7
2 eq.	1.60, ddd, (12.6, 4.1, 2.4)	1.59	1.50			
3	4.16, tt, (12.6, 4.1)	4.35	4.33	73.2	68.6	69.0
4ax.	1.82, dd, (13.2, 12.6)	1.84	2.03	41.4	44.4	46.6
4 eq.	2.12, ddd, (13.2, 4.1, 2.4)	2.07	2.19			
5				81.5	82.4	82.6
6				72.0	75.7	75.7
7α	1.99, m	1.99	1.94	29.9	33.5	33.9
7β	2.34, m	2.25	2.31			
8	4.51, m	4.61	4.60	97.6	96.5	96.5
9				149.4	146.6	146.8
10	1.66, m	1.68	1.58	20.0	21.0	21.0
		1.77	1.73			
		1.54	1.66			
11	1.03, s	0.94	1.06	27.4	28.0	28.2
		0.97	1.27			
		0.96	0.66			
12	1.07, s	1.19	0.61	24.6	25.2	25.3
		1.46	1.59			
		0.68	1.17			
13	1.30, s	0.89	1.60	22.7	25.2	24.8
		1.63	0.98			
		1.49	1.32			
1′	4.43, d, (7.8)	4.54	4.50	102.8	103.9	104.1
2′	3.18, dd, (9.1, 7.8)	3.51	3.51	75.1	76.5	76.6

^{1}H NMR CS values (δ_H)				^{13}C NMR CS values (δ_C)		
Position[a]	**Exp. δ_H, multi, (*J* in Hz)**	**Cal.**			**Cal.**	
		I[b]	**III**[c]	**Exp.**	**I**[b]	**III**[c]
3′	3.39, m	3.74	3.73	78.0	78.1	78.2
4′	3.35, m	3.60	3.56	71.6	72.3	72.2
5′	3.35, m	3.51	3.51	77.8	77.8	78.2
6′a	3.90, dd, (11.9, 2.1)	4.08	4.09	62.7	64.9	65.0
6′b	3.73, dd, (11.9, 5.1)	3.83	3.83			
DP4 (%)		96.3	3.7		70.9	29.1

[a] See Fig. 1A.

[b,c] Calculated CS values for diastereomers **I** and **III** (Fig. 2B), respectively, employing GIAO shielding CS calculation.